Model of 1,1,1,3,3,3-Hexafluoro-propan-2-ol for Molecular Dynamics Simulations

4 **AUTHORS**, INCLUDING:

Marco Fioroni
46 PUBLICATIONS   951 CITATIONS

SEE PROFILE

Danilo Roccatano
University of Lincoln
103 PUBLICATIONS   2,326 CITATIONS

SEE PROFILE

Model of 1,1,1,3,3,3-Hexafluoro-propan-2-ol for Molecular Dynamics Simulations

Marco Fioroni,*,† Klaus Burger,† Alan E. Mark,‡ and Danilo Roccatano*,§

Fakultät für Chemie und Mineralogie, Institut für Organische Chemie, University of Leipzig, Johannisallee 29, 04103 Leipzig, Germany, Groningen Biomolecular Sciences and Biotechnology Institute (GBB), Department of Biophysical Chemistry, University of Groningen, Nijenborgh 4, 9747 AG Groningen, The Netherlands, and Dipartimento di Chimica, Università di Roma "La Sapienza", P.le Aldo Moro 5, 00185 Roma, Italy

An all-atom model of 1,1,1,3,3,3-hexafluoro-propan-2-ol (HFIP) for use in molecular dynamics simulation studies is proposed. The model was parametrized by fitting to the experimental density, pressure, and enthalpy of vaporization of the pure liquid at 298 K. The model was then tested by comparison against other experimental thermodynamic and kinetic properties of the pure liquid. Mixtures with SPC water were also investigated. Overall, reasonable agreement with the available experimental data for the neat liquid and for mixtures with SPC water was found. A tendency for HFIP to cluster in SPC water was observed in qualitative agreement with experimental observations. The effect of HFIP on the secondary structure of peptides was also studied. Two simulations of the peptide Melittin, in pure water and in 30% v/v HFIP, demonstrate the helix stabilizing effect of HFIP.

1. Introduction

Fluorinated alcohols such as 1,1,1,3,3,3-hexafluoro-propan-2-ol (HFIP) and 2,2,2- trifluoroethanol (TFE) are commonly used to study the conformational states of small peptides and proteins. These alcohols have the capability to increase the content of secondary structure (α-helix) in proteins and peptides.[1] The stabilizing effects of these alcohols change according to the size and nature of the alcohol itself.[1] Recent studies[2,3] demonstrate a stronger secondary structure stabilizing effect of HFIP in comparison with TFE. One reason for this effect is related to the low polarity of the solvent.[4] The low polarity of HFIP allows the formation of micro clusters in aqueous solution that could play an important, but as yet not clearly understood, role in the stabilization of the secondary structure of proteins.[3,5,6] The evidence for microheterogeneity in HFIP water mixtures comes primarily from NMR and FTIR studies.[3,7,8] In addition, small-angle X-ray scattering (SAXS) studies indicate that cluster formation is a function of the concentration of the HFIP and that the microheterogeneity reaches a maximum value at a concentration of 30% HFIP by volume.[3] In fact, a direct correlation between the magnitude of the conformational transition induced by HFIP and the extent of cluster formation in water solution is observed, with the maximum helix stabilizing effect also occurring at a HFIP concentration of 30% v/v.[3] To better understand how HFIP stabilizes proteins and peptides, detailed simulation studies using atomic models are necessary. Few such studies of HFIP have, however, been performed. A model of HFIP has been proposed by Kenichi et al.[9] and used to investigate the hydration of this solvent. This model was parametrized by fitting to quantum-mechanical (QM) derived interatomic potentials. Internal degrees of freedom were ne-

glected. The model was shown to reproduce the experimental hydration free energy of HFIP, but other properties such as cluster formation in water were not analyzed. The functional form used to describe the intermolecular interactions in this model is quite different to ones commonly used in force fields designed for the simulation of biomolecular systems which limits the transferability of the model. To our knowledge, no other models of HFIP suitable for use in MD simulations and specifically optimized to reproduce the physicochemical properties of the neat liquid as well as mixtures with water have been published.

In this paper, we propose a simple model of HFIP for use in MD simulations based on the GROMOS96[10] force field. The model was parametrized to reproduce the density, pressure and the vaporization enthalpy of the pure liquid. The physicochemical properties of the optimized model were then compared with a range of other experimental data including the compressibility, the thermal expansion coefficients, and the dielectric constant. The thermodynamic and structural properties of mixtures with SPC[11] water were also calculated and compared with the experimental values. A simulation of an α-helix forming peptide (Melittin[12]) in a 30% v/v HFIP/SPC water mixture was also performed to analyze the effect of the solvent on the structure of a peptide. Melittin, a 26 a.a. amphiphilic peptide from honey bee venom, is largely unstructured in water but adopts an α-helical structure upon addition of HFIP. The circular dichroism ellipticity at 222 nm reaches a maximum at around 10% v/v for a mixture of HFIP/water, with a plateau between 10 and 40%.[3] The simulation of Melittin in the HFIP/water mixture has allowed us to qualitatively verify the helix promoting effect of our HFIP model and to analyze the distribution of HFIP around the solute.

2. Methods

2.1. HFIP Force Field Parameters. All ab initio calculations were performed using the Gaussian 98 package.[13] A geometry optimization of the HFIP molecule at the SCF level was

---

* To whom correspondence should be addressed. Fax: +39−06−490324. E−mail: roccata@caspur.it. Fax:+49-341-9736599. E−mail: fioroni@organik.chemie.uni-leipzig.de. Fax: +31−50−3634800. E−mail: mark@chem.rug.nl.
† University of Leipzig.
‡ University of Groningen.
§ Università di Roma.

TABLE 1: Optimized ab Initio Geometries of the ap and syn Forms of HFIP in Vacuum[a]

	HFIP (syn)	HFIP (ap)
$r(C-C_c)$[b]	0.152	0.152
$r(C-F_1)$	0.135	0.136
$r(C-F_2)$	0.135	0.135
$r(C-F_3)$	0.136	0.135
$r(C_c-H_c)$	0.109	0.109
$r(C_c-O)$	0.142	0.141
$r(O-H)$[b]	0.096	0.096
$\theta(C_c-C-F_1)$[c]	112.9	110.8
$\theta(C_c-C-F_2)$	111.0	111.3
$\theta(C_c-C-F_3)$	110.4	112.3
$\theta(F_1-C-F_2)$	107.6	107.2
$\theta(F_1-C-F_3)$	107.1	107.4
$\theta(F_2-C-F_3)$	107.2	107.2
$\theta(C-C_c-O)$	109.4	109.2
$\theta(C-C_c-C)$	113.9	111.6
$\theta(H_c-C_c-O)$	111.4	105.5
$\theta(C_c-O-H)$	109.0	108.2
$\phi(F_1-C-C_c-H_c)$[c]	176.5	-175.1
$\phi(F_2-C-C_c-H_c)$	55.4	65.5
$\phi(F_3-C-C_c-H_c)$	-63.2	-55.1
$\phi(F_1-C-C_c-C)$	55.9	63.8
$\phi(F_2-C-C_c-C)$	-65.0	-55.5
$\phi(F_3-C-C_c-C)$	176.1	-176.1
$\phi(F_1-C-C_c-O)$	-63.0	-61.5
$\phi(F_2-C-C_c-O)$	175.4	179.0
$\phi(F_3-C-C_c-O)$	56.7	58.3
$\phi(C-C_c-O-H)$	-69.1	69.2
$\phi(H_c-C_c-O-H)$	57.0	-176.7

[a] C_c is the central carbon, H_c is the hydrogen bound to the central carbon, and C is the carbons of the trifluoromethyl groups. The geometrical parameters of the second CF_3 group are not reported due to the symmetry of the molecule. [b] Distances in nm. [c] Angles in degree.

performed using the 6-311++G** basis set. The dihedral angle H−C−O−H (ϕ) defines two different conformers. The synclinal (syn) conformer has a value of $\phi = \pm 60°$. In this conformation, a weak internal hydrogen bonding between a F atom and the hydroxyl hydrogen is present. The antiperiplanar (ap) conformer has the ϕ angle in a staggered position with $\phi = 180°$. In Table 1, the structural parameters optimized for the two conformers obtained from the ab initio calculations are reported. Bond lengths and angles are very similar between the two conformers and were used to define the reference bond lengths and angles for the HFIP model. The values are consistent with those used for the previous parametrization of TFE.[14]

The single-point energies and charge densities were calculated for the optimized structures including electronic correlations at the MP2 level, with the 6-311++G** basis set. This large basis set was necessary to accurately reproduce the energy difference between the conformers.[15] The energy difference between the two conformers is 3.5 kJ mol^{-1} with the ap conformer being lower in energy. Another ab initio study using density functional theory at the B3LYP/6-31+G* level gave a slightly larger difference of 5 kJ mol^{-1}.[7] The calculated data are in excellent agreement with the experimental value of 4 ± 1 kJ mol^{-1}, measured in the gas phase by Hollenstein et al.[16] Studies of liquid HFIP and HFIP in CCl_4, however, indicate an energy difference between the two conformers of only 0.4 kJ mol^{-1}.[17] Spectroscopic data are consistent with the existence of a loose internal H···F hydrogen bond in liquid HFIP,[7] giving as the most populated conformer the ap form. Ab initio calculations on HFIP dimers and trimers[7] have shown that the most stable structures are those with a hydrogen bond between two HFIP molecules in ap form.

The partial atomic charges were obtained using the CHELPG procedure.[18] This procedure has been shown to give reasonable

TABLE 2: Summary of Charges Derived from Quantum-Mechanical Calculations of the Two HFIP Conformers in Vacuum[a]

atom type	HFIP (syn)	HFIP (ap)	differences
C	0.848	0.806	0.042
F	−0.252	−0.249	−0.003
F	−0.264	−0.249	−0.015
F	−0.285	−0.265	−0.020
C_c	−0.079	-0.169	0.090
H_c	0.163	0.208	−0.045
C	0.762	0.802	−0.040
F	−0.249	−0.248	−0.001
F	−0.262	−0.264	0.002
F	−0.229	−0.248	0.019
O	−0.567	−0.534	−0.033
H	0.414	0.412	0.002
dipole	1.583	0.634	

[a] The units of the charge and the dipole are electrons and debye, respectively.

partial charges for use in MD force fields.[19] In Table 2, the charges obtained from the MP2 calculations on the two conformers are reported. The largest deviations between the two conformers occur on the central carbon with the deviations within the asymmetric ap form in fact greater than those between the ap and syn forms. The LJ parameters for the non fluorine atoms have been taken from the GROMOS96 force field and the initial estimates for the charges from the MP2 calculations on the optimized ap form. This choice is a consequence of the fact that the ap form is the dominate fraction in the gas phase.[7] The differences in the partial charges between the two conformers are, as noted above, relatively small.

The use of dihedral potential functions to fit the potential energy surface obtained from ab initio calculations prevented the simultaneous reproduction of both thermodynamic and dynamical liquid properties. The stabilization of the syn form using additional dihedral potentials reduced drastically the mobility of the molecules. For this reason, our model has no torsional potential functions on all of the dihedrals. Therefore, the model does not reproduce the difference in energy between the ap and syn conformer obtained from in-vacuum ab initio calculations. The model was optimized to reproduce the liquid properties of HFIP, in particular the density at atmospheric pressure and the enthalpy of vaporization at 298 K.

The LJ interaction parameters between two atoms were calculated as the geometric mean of the LJ parameters of the corresponding atom types; that is, $C_{1,2}^{\alpha} = \sqrt{C_{1,1}^{\alpha} C_{2,2}^{\alpha}}$ with $\alpha = 12$ or 6 and index 1 or 2 referring to the different atom species. Starting from this set of nonbonded parameters, systematic changes of the partial charges of all atoms and LJ parameters of the F atoms were made. Details of the simulations are reported in the next session.

Initially the LJ parameters for the fluorine atom were taken from our previous parametrization of TFE. Using those parameters, however, it was not possible to reproduce the experimental enthalpy of vaporization and the density unless the standard GROMOS96 parameters for non fluorine atoms were modified. To maintain the consistency of the force field, a new fluorine atom type was therefore defined for the HFIP model. In Table 3, the optimized parameters for HFIP are reported.

2.2. MD Simulations. Different simulations of pure HFIP and mixtures with SPC water were performed. The neat liquid was simulated at three different temperatures under NpT and NVT conditions using a periodic simulation box containing 400 molecules. A system containing 648 HFIP molecules was also simulated using a reaction-field correction to the long-range

Model of 1,1,1,3,3,3-Hexafluoro-propan-2-ol

J. Phys. Chem. B, Vol. 105, No. 44, 2001 **10969**

TABLE 3: Force Field Parameters for the HFIP Model

atom type	$C^6_{i,i}/$ (kJ mol^{-1} nm^6) $\times 10^3$	$C^{12}_{i,i}/$ (kJ mol^{-1} nm^{12}) $\times 10^6$	q/e
F	1.177862	1.168000	−0.200
C	2.340624	3.374569	0.600
C_c	2.340624	3.374569	−0.070
H	0	0	0.495
H_c	0.084640	0.015129	0.170
O	2.261954	1.505529	−0.595

bond	distance (nm)
C−F	0.136
C_c−C	0.153
C_c−O	0.136
C_c−H_c	0.109
O−H	0.100

bond angle	θ_0 (degrees)	K_θ (kJ mol^{-1} rad^{-2})
C−C_c−O	111.0	460.2
C−C_c−H_c	109.5	460.2
C−C_c−C	111.0	460.2
F−C−F	107.6	460.2
F−C−C_c	111.0	460.2
C_c−O−H	109.5	397.5
O−C−H_c	109.5	397.5

TABLE 4: Summary of the Simulations of the Pure HFIP^a

T^b	sim. time^c	N_{HFIP}	conditions	ρ^d	p^e	ΔH_{vap}^f
293	2	400	NpT	1.62	1.0	42.10
293$_{RF}$	5	648	NpT	1.61	1.0	41.50
298	2	400	NpT	1.60	1.0	41.68
298	2	400	NVT	1.60	2.5	41.68
313	2	400	NpT	1.56	1.0	37.90
313	2	400	NVT	1.56	5.0	37.90
exp						
293			NpT	1.62	1.0	42.76
298			NpT	1.60	1.0	41.58
313			NpT	1.56	1.0	38.98

^{a} The subscript RF denotes the simulation performed using the reaction field. The standard deviations of computed values are 0.01 kg m^{-3}, 300 bar, and 0.4 kJ mol^{-1}, for the density, pressure, and vaporization enthalpy, respectively. ^{b} K. ^{c} ns. ^{d} (kg m^{-3}) $\times 10^{-3}$. ^{e} bar. ^{f} kJ mol^{-1}.

TABLE 5: Calculated (calc) and Experimental (exp) Thermodynamic and Kinetic Properties of Pure HFIP at 298 K^a

	β_T^b	α (der)^c	α (fluc)^c	ϵ_r	η^d
calc	0.8	1.47	0.55	8.5	2.58
exp	2.03	1.59	1.59	17.8	1.58

^{a} For the dielectric constant the temperature is 293 K. For the thermal expansion coefficient the value obtain from eq 4 (der) and from eq 5 (flu) are reported. ^{b} (bar^{-1}) $\times 10^4$. ^{c} (K^{-1}) $\times 10^3$. ^{d} (kg m s^{-2}) $\times 10^3$.

electrostatic interactions in order to determine the dielectric properties of the model. The parameters used for the simulations are reported in Table 4. In the case of the mixtures, 10 different NpT simulations at 298 K were performed. Furthermore, seven of these mixture simulations (see Table 7) were performed at 293 K, with reaction-field correction, to calculate the dielectric properties and compare them with the available experimental data. In Table 6, the composition of each of the mixed systems simulated is reported. In all simulations, the temperature was maintained close to the reference value by weak coupling to an external temperature bath[20] with a coupling constant of 0.01 ps. In the constant pressure simulations, the pressure was maintained by weak coupling to an external pressure bath of $P_0 = 1$ bar.[20] Using the experimental value of the compressibility of HFIP (2.03×10^{-4} bar^{-1})[21] in the simulation of the neat

TABLE 6: Thermodynamic Properties of HFIP/Water Mixtures at 298 K^a

x_{HFIP}	sim. time^b	N_{HFIP}	N_w	v/v	ρ^c	p^d	$\Delta H_{mix}^{calc\ e}$	ΔH_{mix}^{exp}
0.000	2	0	1074	0	0.99	1.0	0.00	0.00
0.020	2	30	1435	10	1.11	1.1	0.10±0.16	−0.20
0.082	2	100	1117	34	1.18	1.0	0.33±0.16	−0.38
0.133	2	150	979	47	1.25	0.9	0.41±0.19	−0.41
0.222	2	200	700	62	1.32	0.6	0.69±0.21	−0.50
0.359	2	250	445	76	1.40	0.7	0.19±0.27	−0.52
0.409	2	300	432	80	1.43	0.9	0.09±0.25	−0.60
0.552	2	300	243	87	1.47	1.0	−0.49±0.37	−0.48
0.662	2	350	178	92	1.51	0.7	−1.05±0.38	−0.46
0.795	2	350	90	96	1.55	1.2	−0.90±0.43	−0.40
0.897	2	350	40	98	1.57	1.0	−0.29±0.47	−0.28
1.000	2	400	0	100	1.60	1.0	0.00	0.00

^{a} The standard deviation for the calculated density and pressure values are 0.01 kg m^{-3} and 300 bar, respectively. The errors for the calculated mixing enthalpies are reported directly in the table. ^{b} ns. ^{c} (kg m^{-3}) $\times 10^{-3}$. ^{d} bar. ^{e} kJ mol^{-1}.

TABLE 7: Experimental (exp) and Calculated (calc) Dielectric Constants of HFIP/Water Mixtures at 293 K^a

x_{HFIP}	v/v	ϵ_{exp}	ϵ_{calc}	D_{HFIP}^b	D_{SPC}^b
0.000	0	80.1	63.5		4.1 ± 0.2
0.020	10	71.3	60.5	3.2 ± 0.2	3.4 ± 0.2
0.082	34	56.9	41.1	2.2 ± 0.2	2.5 ± 0.2
0.133	47	51.0	32.5	1.3 ± 0.3	2.1 ± 0.2
0.409	80	30.3	23.0	0.6 ± 0.2	0.9 ± 0.2
0.662	92	24.0	15.0	0.2 ± 0.3	0.2 ± 0.2
1.0	100	17.8	8.5	0.06 ± 0.01	

^{a} Diffusion coefficients are calculated at 298 K. The number of molecules in the boxes used for the calculations are the corresponding ones at the same molar fractions as those in Table 6. ^{b} 10^{-5} cm^2 s^{-1}.

liquid, a coupling constant of $\tau_P = 8$ ps was required. This reflects the fact the model underestimates the compressibility of pure HFIP. Simulations of the mixtures were performed using the experimental compressibility of pure water (4.5×10^{-5} bar^{-1}), and as a consequence, a coupling constant of $\tau_P = 1$ ps could be used.[20]

The LINCS algorithm[22] was used to constrain all bond lengths in HFIP. For the water molecules, the SETTLE algorithm was used.[23] A twin-range cutoff for the calculation of the nonbonded interactions was applied. All interactions within a short range cutoff of 0.8 nm were updated every step, whereas all interactions (Coulomb and Lennard-Jones) within a long range cutoff of 1.4 nm were updated only every 5 steps together with the pair list. The cutoff values are in accord with those standardly used in the GROMOS96 force field.[10] A dielectric permittivity of $\epsilon_r = 1$ and a time step of 2 fs were used. In simulations with reaction-field correction, the value of ϵ_{RF} was set to the experimental dielectric permittivity of the simulated system (see Table 7).

Before starting the simulations, the systems were first minimized for 100 steps using the steepest descent algorithm to eliminate unfavorable contacts. Initial velocities were assigned from a Maxwellian distribution corresponding to the selected temperature. For the relaxation and equilibration of the systems, simulations of 100 ps long were conducted. After equilibration, simulation runs of 2 ns long were performed for the analysis.

Thermodynamic properties were obtained either from the second moment of the central distribution of an appropriate thermodynamic variable[24] or from two simulations of the system at two thermodynamic states using numerical derivatives. When estimating thermodynamic quantities from the second moment of the distribution, two potential problems have to be considered. One is the reliability of the method used to generate the

simulated ensemble. In particular, the weak coupling method used to maintain the temperature and pressure in the simulations does not exactly reproduce a canonical ensemble.[25] The second is that the second moments can be slow to converge. Long simulation times are required to obtain reliable results. The dielectric constant for the liquid was estimated from the fluctuation of the total dipolar moment. Therefore, to obtain convergence, longer simulations were performed for this calculation. The errors associated with the average properties were calculated using the block averaging method described previously.[24]

2.3. MD Simulations of the Melittin Helix in the HFIP/ SPC Mixture. The starting conformation for the simulations of the Melittin peptide was taken from the 0.2 nm resolution crystal structure (pdb-entry: 2MLT).[26] The peptide was protonated such that N-terminal NH_3^+ and C-terminal COO^- groups were in accord with the experimental conditions. The peptide was centered in a cubic box of 5 nm in edge and solvated with either pure SPC water molecules or a mixture of SPC water and HFIP molecules. The protonation state of the peptide at pH 3 gives a total charge of +5. A number of Cl^- counterions were therefore added to each system to reduce the overall charge on the system. This was achieved by replacing water molecules at the most positive potential. The results discussed in the text correspond to 5 ns simulations performed using 3 counterions. Shorter simulations incorporating 5 counterions yielded, however, essentially identical results. All solvent molecules with any atom within 0.15 nm of the peptide were removed. The final systems contained either 3780 SPC water molecules or 2150 SPC water and 157 HFIP molecules (corresponding to approximately 30% v/v). After equilibration, the box lengths were approximately 4.8 and 4.6, respectively. The GROMOS96 force field[10] was used to describe the peptide. All bond lengths in the peptide were constrained using the LINCS[22] algorithm.

GROMOS96 specifically optimize cross LJ interaction parameters between non-fluorine HFIP and peptide atoms, which have been used during the simulations. For the fluorine atom LJ interactions, GROMOS96 combination rules were used to generate a new set of cross pair interaction parameters with the peptide atom types.

The simulations were performed at 298 K under NpT conditions using the procedure described above for the HFIP/ water mixture simulations. The system was first minimized using a steepest descent algorithm, followed by 150 ps of MD with position restraints on the peptide to allow the relaxation of the solvent molecules. This was followed by another 50 ps of equilibration without position restraints. Simulations of 5 ns were then performed for analysis.

Cluster analysis was performed using the Jarvis–Patrick[27] method: a structure is added to a cluster when this structure and a structure in the cluster have each other as neighbors and they have at least P neighbors in common. The neighbors of a structure are the M closest structures or all of the structures within a cutoff, based on the root means squared deviation (RMSD) between backbone atoms. In our case P was 3, M was 10, and the RMSD cutoff was 0.1 nm. All simulations and trajectory analysis were performed using the GROMACS2.0 software package in double precision.[28]

3. Physico-Chemical Properties of Pure HFIP

3.1. Structural Properties. In pure HFIP and in CCl_4, the energy difference between the ap and syn conformers is in the order of 0.4 kJ mol^{-1}.[17,7] From the distribution of the HCOH
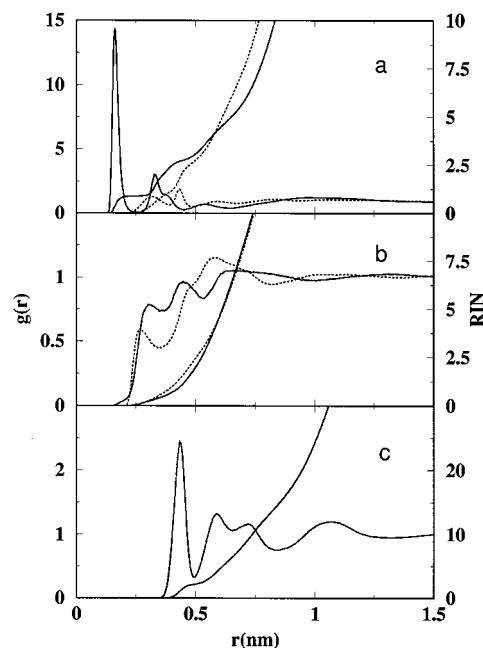

Figure 1. Radial distribution functions (RDF) between specific pairs of atoms derived from molecular dynamics (MD) simulations of pure 1,1,1,3,3,3-hexafluoro-propan-2-ol(HFIP) at 298 K: (a) O–H$_c$, dotted lines and O–H, solid lines; (b) F–H, solid line and F–H$_c$, dotted line; (c) C$_c$–C$_c$, solid line. Curves indicating the running integration number (RIN) for each pair are also shown using the same line coding.

dihedral angle in the simulation of liquid HFIP, a free energy difference of $\Delta G = 1.7$ kJ mol^{-1} was obtained.

The intermolecular radial pair distribution functions (RDFs),[24] denoted by $g_{xy}(r)$ and calculated from the simulation at 298 K, for different pairs of atoms, are shown in Figure 1. In the same figure, the running integration number (RIN)

$$n_{xy} = 4\pi\rho_0 \int_0^R g_{xy}(r)r^2 \, dr \tag{1}$$

where ρ_0 is the number density of the atoms of kind y, is reported. The RIN give the average number of atoms y contained in a sphere of radius R centered on atom x.

In Figure 1a, the $g(r)$ functions between the pairs O–H and O–H$_c$ are reported (only intermolecular contributions are shown). The $g_{OH}(r)$ function shows a sharp peak at a distance of 0.16 nm and a RIN of 1.0 denoting the presence of a hydrogen bond interaction. The second peak at 0.33 nm (RIN = 2) originates from the hydroxyl hydrogen of the acceptor molecules. In Figure 2, a snapshot of one frame of the trajectory shows the spatial arrangement of the HFIP molecules. Hydrogen bonding interactions, indicated in Figure 2 by broken lines, were geometrically defined. A hydrogen bond was considered to exist if the distance between O···H was less than 0.25 nm and the corresponding angle O–H···O was greater than 60°. The average number of hydrogen bonds per HFIP molecule was two (considering the oxygen as both a donor and an acceptor). From the figure, it is evident that the CF$_3$ groups show a tendency to cluster.

There is some experimental evidence[7] indicating a weak intramolecular interaction between the fluorine and the hydroxyl hydrogen of HFIP in both the vapor and the liquid. That this is mimicked in the simulations is evident in Figure 1b where the $g_{FH}(r)$ shows a peak at 0.30 nm with a RIN equal to 0.3. The $g_{FHc}(r)$ function (Figure 1b), where H$_c$ is the hydrogen of the central carbon, shows a similar peak at 0.27 nm with a RIN of 0.4. The values of these distances are very close to those

Model of 1,1,1,3,3,3-Hexafluoro-propan-2-ol

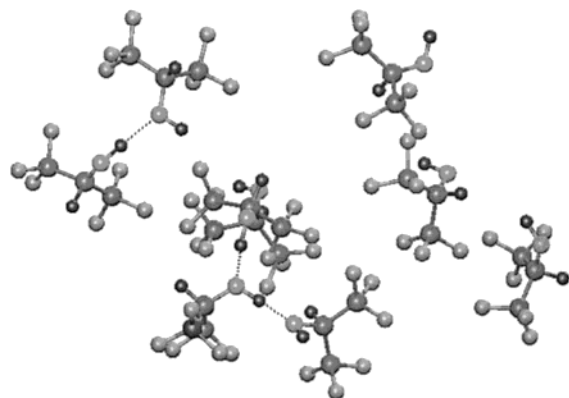*J. Phys. Chem. B, Vol. 105, No. 44, 2001* **10971**

Figure 2. Example of a cluster of HFIP molecules present in the simulations of the pure liquid. Dotted lines indicate hydrogen bonds.

predicted for stable dimers in a vacuum obtained from quantum-mechanical calculations.[7]

Finally, the long-range structure of the liquid is indicated by the g_{CcCc}function (Figure 1c). The oscillating behavior of the g_{CcCc}function is evidence of long-range structural order produced by the hydrogen bond interactions and the clustering of the hydrophobic CF_3 groups. The first peak at 0.43 nm has a RIN equal to 2, as expected from the analysis of the $g_{OH}(r)$ function. In the second shell (0.50−0.87 nm), the number of coordinating molecules is approximately 13.

3.2. Thermodynamic Properties. Different thermodynamic properties of pure HFIP have been calculated. The thermodynamic properties used to optimize the HFIP model were the density,[29] the pressure, and the enthalpy of vaporization at 298 K. The other properties calculated were used as controls in order to verify the model. In Table 4, a comparison between the calculated and the experimental values for the density, pressure, and enthalpy of vaporization is reported. The density at 1 atm and 298 K is within 0.1% of the experimental value. The enthalpy of vaporization is identical to within 4 significant figures under NVT or NpT conditions. The enthalpy of vaporization deviates slightly at 293 and 313 K from the experimental values.

The pressure is very sensitive to the simulation conditions, in particular to changes in the cutoff radius. A reduction of the long-range cutoff radius from 1.4 to 1.2 nm results in a change in the average pressure of 100 bar. Other properties remain practically unchanged. This effect has been also shown with other solvents.[14,30] A strong box size dependence was observed. In systems containing less than 230 molecules, the pressure (NVT), the density (NpT), and the total dipole were strongly dependent on the number of molecules because of long range ordering induced by the PBC.

The heat of vaporization was estimated as

$$\Delta H_{vap} = [U_{inter}(g) - U_{inter}(l)] + [U_{intra}(g) - U_{intra}(l)] + RT \quad (2)$$

where $U_{inter}(g)$ is the total potential energy for the interatomic nonbonded interactions and U_{intra} is the intramolecular energy (angles, torsions, and intramolecular nonbonded interactions). $U_{inter}(g)$ was assumed to be zero, whereas $U_{intra}(g)$ was calculated by averaging over a number of independent simulations of isolated molecules. The error in the enthalpy is 0.24% at 298 K. In Table 5, other thermodynamic and kinetic properties calculated, together with the corresponding experimental values, are reported.

The isothermal compressibility β_T was estimated from the finite difference relationship

$$\beta_T = -\frac{1}{V}\left(\frac{\delta V}{\delta P}\right)_T = \frac{1}{\rho}\left(\frac{\delta \rho}{\delta P}\right)_T = \left(\frac{\delta \ln \rho}{\delta P}\right)_T \approx \left(\frac{\ln\left(\frac{\rho_2}{\rho_1}\right)}{P_2 - P_1}\right)_T \quad (3)$$

where ρ_1 and ρ_2 and P_1 and P_2 are, respectively, the densities and the pressures obtained from two simulations at the same temperature but different pressures. The difference in pressure was obtained by reducing the box volume by 0.5%. The value calculated at 298 K was 0.8×10^{-4} bar^{-1} which is a factor 2 less than the experimental value of 2.04×10^{-4} bar^{-1}.[21]

The thermal expansion coefficient was evaluated using the following numerical derivative:

$$\alpha = \frac{1}{V}\left(\frac{\delta V}{\delta T}\right)_P \approx -\left(\frac{\ln\left(\frac{\rho_2}{\rho_1}\right)}{T_2 - T_1}\right)_P \quad (4)$$

and also estimated from the fluctuations in the volume of the system using the relation[24]

$$\alpha = \frac{\langle \Delta H \Delta V \rangle}{\langle V \rangle k T^2} \quad (5)$$

where H is the "instantaneous enthalpy" of vaporization and V is the volume. For the calculation of this value, simulations at two different temperatures at 298 and 313 K were performed.

The value calculated using eq 4 between 298 and 313 K was 1.47×10^{-3} K^{-1}. This is very close to the experimental value of 1.59×10^{-3}K^{-1}.[31] The value of α calculated from the fluctuation formula was 0.55×10^{-3} K^{-1}. Most likely this difference is in part due to the temperature and pressure coupling schemes used. The tight coupling constants used may have suppressed the fluctuations in the system. Longer simulations might also be required to obtain convergence when using the fluctuation formula.

3.3. Dynamical Properties. *Tracer Diffusion Coefficients.* The tracer diffusion coefficients (D) were calculated using the Einstein relation[24] from the slope of the center of mass mean square displacement (msd) of HFIP molecules. The msd was calculated for each HFIP molecule in the simulation box. Multiple starting points (each every 50 ps) were used to evaluate the msd curve. The use of well separated starting points improves the statistics of the curve and reduces the effects of correlations on the computed value of D.[24] The resulting average msd curve was used to estimate the slope by linear regression. In the regression, the first 5 ps of the msd curve, which contains the collisional part of the diffusion curve, was neglected. The calculated value of D at 298 K was 0.06×10^{-5}cm^2 s^{-1}. Unfortunately, to our knowledge, no experimental data are available for a direct comparison.

Static Relative Permittivity. The static relative permittivity, ϵ_r, of pure HFIP was calculated from the fluctuation of the total dipole moment $\langle M^2 \rangle$ of the system using the following equation:[32]

$$(\epsilon_r - 1)\left(\frac{2\epsilon_{RF} + 1}{2\epsilon_{RF} + \epsilon_r}\right) = \frac{\langle M^2 \rangle - \langle M \rangle^2}{3\epsilon_0 V k_B T} \quad (6)$$

where ϵ_r is the relative permittivity used in the reaction field treatment, V is the volume of the box, k_B is the Boltzmann constant, and T is the absolute temperature. Because the
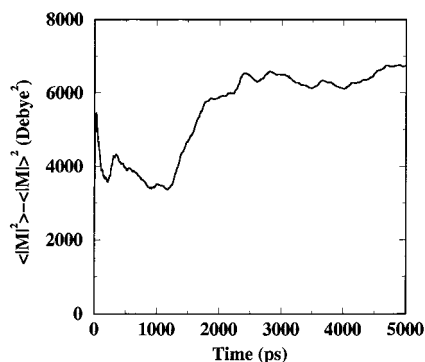
Figure 3. Cumulative average of the fluctuation in the total dipole moment as a function of time obtained from a simulation of liquid HFIP at 293 K performed with reaction field corrections.

fluctuation the $\langle M^2 \rangle$ term converges very slowly, long simulations (up to 5 ns) using a box of 648 HFIP molecules and a reaction field correction to the long-range interactions were performed at 293 K. In Figure 3, the cumulative average of the fluctuation in the total dipole moment of the system versus time is reported. The resulting dielectric constant of 8.5 is lower than the experimental value[3] (17.8). We note, however, that similar differences have been found for other comparable solvents.[33] The effect of different values of ϵ_{RF} on ϵ_r was tested by performing simulations with different values of ϵ_{RF} in a range of 8−28. No significant effect on the final result was observed. It is possible that 5 ns is insufficient to obtain converged results, but it is unlikely that this could account for the observed discrepancy. More likely, the difference between the calculated and experimental values is due the lack of atomic polarizability in the model.

Shear Viscosity. The shear viscosity was calculated at 298 K using the method described by Berendsen.[34,35] In this method, the viscosity of the liquid is estimated from nonequilibrium simulations in which an external shear-stress acceleration field of the form

$$a_{i,x} = A \cos\left(\frac{2\pi z_i}{l_z}\right) \quad (7)$$

with $a_{i,x}$ being the acceleration in the x direction, A the acceleration amplitude, z_i the z coordinate of the particle, l_z the length of the box in the z direction, is applied to the system. The external acceleration field induces a velocity gradient of the same shape. Under these conditions, for a classical (Newtonian) fluid, the dynamic viscosity (η) is simply given by

$$\eta = \frac{A}{v}\sigma\left(\frac{l_z}{2\pi}\right)^2 \quad (8)$$

where σ is the density of the system and vis is the resulting velocity amplitude. A careful choice of the parameter A as well as of the box edge in the z direction (see ref 35) was made in order to induce a perturbation to the system that can be discernible from thermal velocities but still small enough to prevent the appearance of order in the fluid. A rectangular box of $4.9 \times 4.9 \times 9.8$ nm and a value for A of 0.02 nm ps^{-2} was used. The values of v were calculated as described in refs 34 and 35. The value of η obtained from the simulations was 2.58 $\times 10^{-3}$ Kg m s^{-2} at 298 K. The corresponding experimental value[36] is 1.58×10^{-3} Kg m s^{-2}, at the same temperature.

4. Physicochemical Properties of Water-HFIP Mixtures

4.1. Structural Properties. In Figure 4, the $g_{xy}(r)$ functions for the pairs H_w−O, O_w−H, and O−H are reported. The sharp
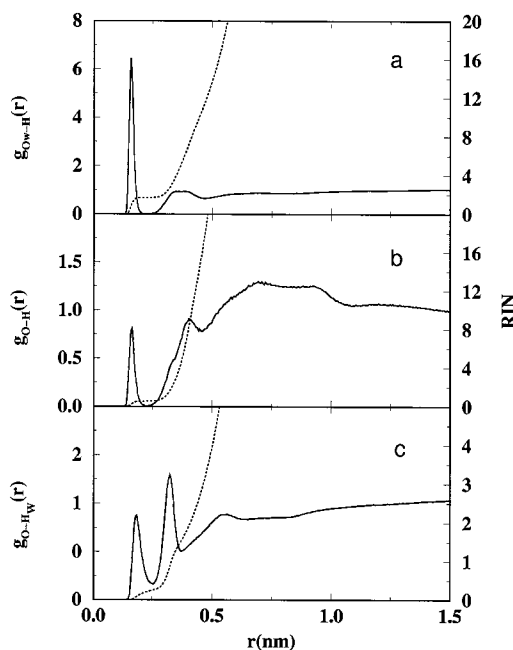

Figure 4. RDF pair distribution functions (solid lines) derived from a MD simulation of a 34% v/v mixture of HFIP in SPC water at 298 K: (a) O_w−H, (b) O−H, and (c) H_w−O. The dotted lines show the corresponding RIN curves.

maximum of the $g_{OwH}(r)$ at a distance of 0.16 nm with a RIN of 1.5 denotes a strong hydrogen bonding interaction between the two species. The $g_{OHw}(r)$ has a first peak at 0.18 nm with a RIN of 0.2 and a second well-defined peak at 0.32 with a RIN of 2. The $g_{OH}(r)$ function shows a sharp peak at 0.16 nm with a RIN of 0.5. Comparing the number of hydrogen bonds between the water and the HFIP molecules, it seems that hydrogen bonding interactions are mainly formed with water. In Figure 5, a snapshot of a box of the HFIP/SPC water mixture, corresponding to a 34% v/v HFIP solution is shown.

The picture clearly shows the microheterogeneity of the solution and cluster formation. The microheterogeneity between the two species can be explained by the tendency of the CF$_3$ groups to cluster, minimizing their contact with water, and by the formation of a network of hydrogen bonds between the HFIP molecules. X-ray scattering measurements[3] of HFIP/water mixtures, having a volume concentration of HFIP varying between 25 and 35%, suggest there is a strong tendency for the alcohol to cluster with a maximum at around the 30% in volume. To investigate the microheterogenity in the HFIP/water mixtures, the $g_{CcCc}(r)$ for the different HFIP/water mixtures were calculated and compared to that of the pure liquid. In Figure 6, the RDFs are reported. The sharp first peak at 0.43 nm, observed in the pure liquid, progressively diminishes with increasing water concentration. This effect is a consequence of the water molecules interfering the formation of HFIP dimers. The structure observed in the pure liquid in the range 0.50−0.9 nm remains present, although the two peaks broaden and become less well defined (Figure 1c). The relative positions of the two peaks remain unchanged at 0.53 and 0.70 nm, respectively. The value of the RIN at 0.9 nm increases going from the lowest to the highest HFIP concentration, with values of 5.2, 6, 9.5, and 17 for the 10%, 34%, 42%, and 62% mixtures, respectively. These values may be compared with that of the pure liquid which has a RIN at 0.9 nm also of 17. The fact that the RIN value does not scale linearly with the percentage HFIP is further evidence of cluster formation.
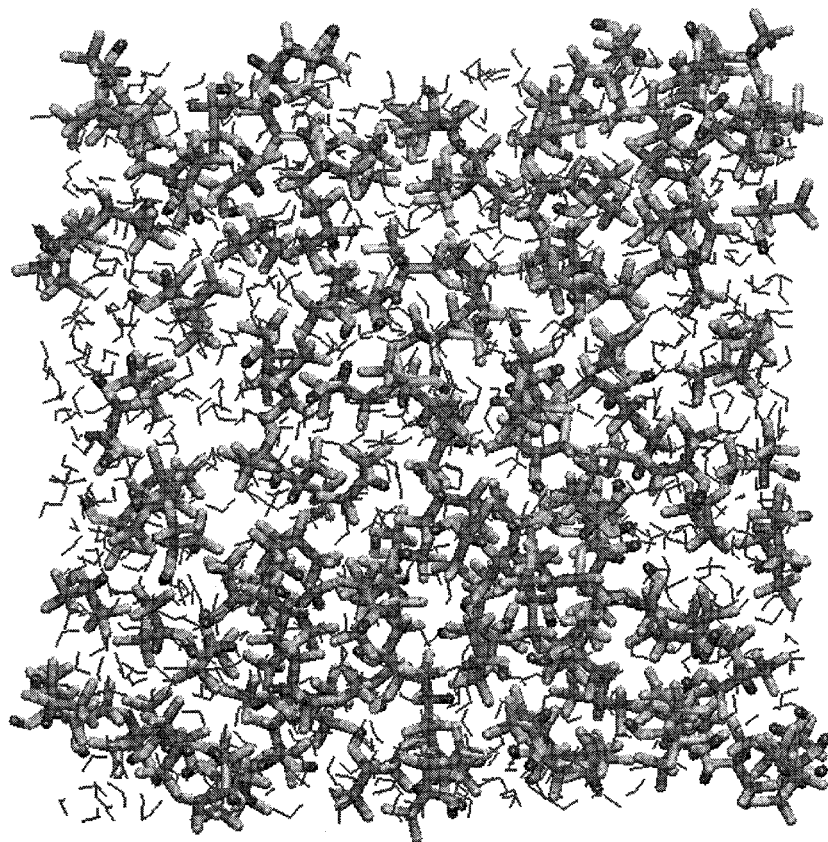
Model of 1,1,1,3,3,3-Hexafluoro-propan-2-ol

J. Phys. Chem. B, Vol. 105, No. 44, 2001 **10973**

Figure 5. Snapshot after 2 ns from a simulation of a 34% v/v HFIP/water mixture. The HFIP molecules are presented in a tube representation, whereas the water is shown in a wire representation.
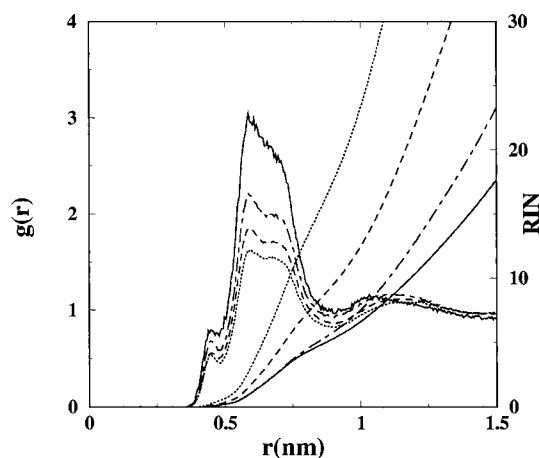

Figure 6. Pair distribution functions between C_c atoms derived from simulations of HFIP/water mixtures: 10% (solid line), 34% (dot−dashed), 42% (dashed), and 62% (dotted) in v/v in HFIP. The running integration numbers are plotted with the same symbol as the corresponding RDF function.

4.2. Thermodynamic and Dynamical Properties. *Hydration Free Energy.* The hydration free energy was estimated using the thermodynamic integration method.[37] In this approach, the Hamiltonian (H) of the system is made a function of a coupling parameter λ which when $\lambda = 0$ the system corresponds to state A and when $\lambda = 1$ the system correspond to state B. In this way, the change in free energy can be calculated by

$$\Delta F_{BA} = \int_0^1 F'(\lambda) \, d\lambda = \int_0^1 \left\langle \frac{\partial H}{\partial \lambda} \right\rangle d\lambda \tag{9}$$

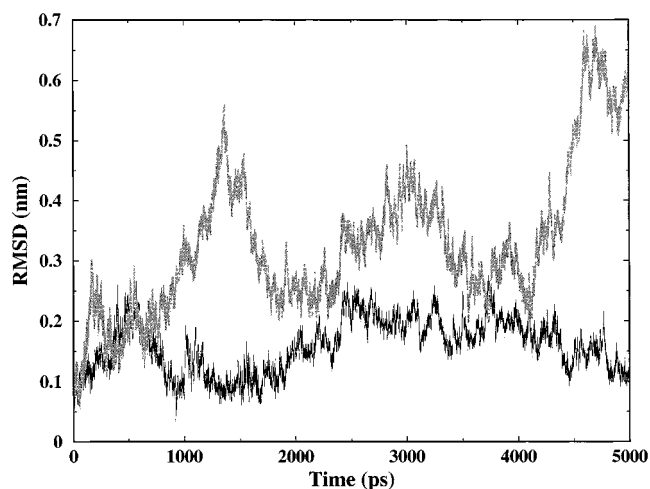where the angular brackets $\langle \rangle$ denote averaging over an

Figure 7. Main chain RMSD of the Melittin from the water (thick gray) and 30% HFIP/water (solid) simulations.

equilibrium ensemble generated with $H(\lambda)$. The integral in eq 9 was evaluated by obtaining ensemble averages over 23 discrete λ points and determining the integral numerically. At each λ point, 50 ps of equilibration and 150 ps of sampling was performed. Numerical instabilities that can occur during the disappearance of atoms were avoided by using a soft-core interaction function[38,39] as described by Daura et al.[40] The hydration free energy (ΔG_{hydr}) was calculated by deleting a HFIP molecule in a box of 819 SPC water molecules. In this case, the calculation was performed by switching off the nonbonded interactions between the HFIP molecule and the water molecules. The simulations were performed at constant pressure and at 298 K. A value of -17 ± 3 kJ mol^{-1} was obtained from
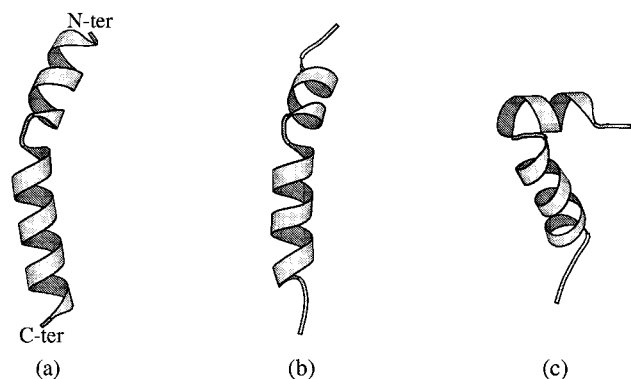
Figure 8. Tertiary structure of the main chain of Melittin: (a) crystal structure, (b) the structure after 5 ns from the HFIP/water simulation, and (c) the structure after 5 ns from the simulation in water. The pictures were obtained using molscript.[48] The secondary structure definitions are based on the Kabsch−Sander DSSP definition.[49]

the calculations which is in very good agreement with the experimental value[41] of −15.8 kJ mol^{-1}.

Mixing Enthalpy and Dielectric Constant. The molar enthalpy of mixing is defined as

$$\Delta H_{mix} = U_{mix} - x_{HFIP}U_{HFIP} - (1 - x_{HFIP})U_{SPC} + p\Delta V_M \quad (10)$$

where U_{mix} is the potential energy of the mixture and U_{HFIP} and x_{HFIP} is the molar fraction of HFIP and U_{SPC} is the potential energy of pure HFIP and pure water, respectively. $U_{HFIP} = 579.75$ kJ mol^{-1} and $U_{SPC} = -42.3$ kJ mol^{-1} have been used in the calculations. The $p\Delta V_M$ contribution to ΔH_{mix}, where V_M is the volume change upon mixing and p the pressure of the solution, was found to be negligible. In Table 6, the experimental[42] and calculated values of mixing enthalpies at the different concentrations of HFIP are reported. The mixing enthalpy is calculated from a difference of two large numbers and is thus very sensitive to the details of the simulation. Despite the careful regulation of the temperature of the system and the use of a time step of 1 fs, the model failed to reproduce the experimental mixing enthalpies at low molar fractions of HFIP. The precise reason for this is unclear. Similar trends have been observed with other solvents and may be related to the use of combination rules to derive HFIP−SPC interactions.[43−45] The

effect may also indicate a slight underestimation of the intermolecular F···H$_w$ interaction which is believed to play an important function in the stabilization of the liquid mixtures.[7] The dielectric constant as a function of composition was calculated as described previously for the pure liquid. The calculations were performed at 293 K for comparison with the available experimental data measured at this temperature. The results are shown in Table 7 together with values obtained experimentally.[3] It is evident that for all mixtures the dielectric while showing the expected trend is systematically underestimated. This further suggests atomic polarizability could play a major role in this discrepancy.

Tracer Diffusion Coefficient. In Table 7, tracer diffusion coefficients for HFIP/SPC water mixtures are reported. Unfortunately, to our knowledge, no experimental data are available for comparison. However, it is to note that the D values increase at low HFIP concentrations. A similar tendency was also observed for other alcohols[46] and a correlation with the dimensions of the molecule was proposed as explanation.[46]

4.3. Melittin Simulation in HFIP/SPC Mixture. In Figure 7, the main-chain root-mean-square deviation (RMSD) of the peptide in pure water and in HFIP/water mixture with respect the crystallographic structure is shown. The peptide never deviates more than 0.25 nm from the starting structure during 5 ns of simulation in the HFIP/water mixture, returning to within 0.1 nm of the starting structure at the end of the simulation. In contrast, the RMSD of the peptide in water rises rapidly to 0.3 nm and shows large oscillations throughout the simulation. Similar results for Melittin in water have also been obtained in recent work by Lin et al.[47] Cluster analysis based on the backbone RMSD was used to analyze the conformations sampled. The HFIP/water simulation showed a single large cluster incorporating 76% of the trajectory with an average deviation from the crystallographic structure of 0.14 nm. In the case of water simulation, 23 clusters were obtained with the three largest incorporating 20, 19, and 16% of the trajectory with average deviations from the starting structure of 0.23, 0.45, and 0.42 nm, respectively. The difference in conformational flexibility of Melittin in water as opposed to the HFIP/water mixture is illustrated in Figure 8. Figure 8 shows for comparison the starting crystallographic structure, the structure after 5 ns from the simulation in 30% v/v HFIP, and the structure after 5 ns from the simulation in water. The structure in HFIP is
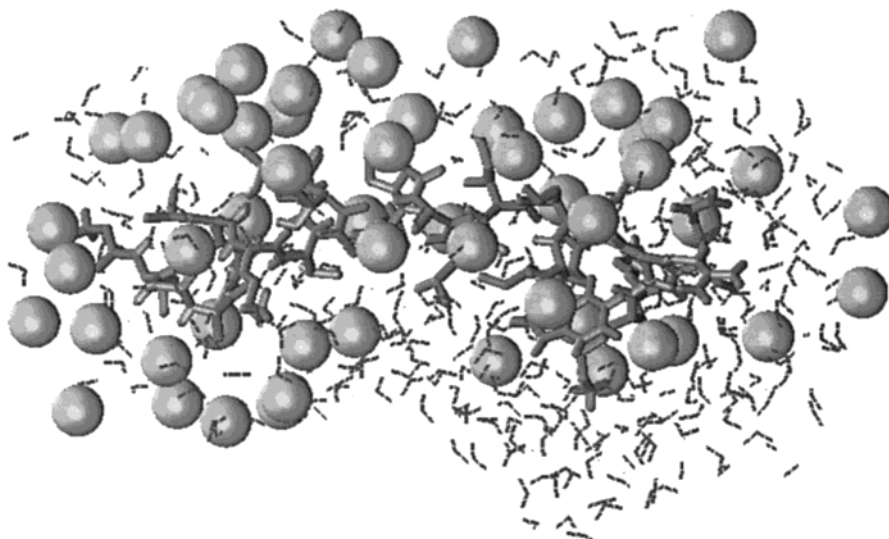

Figure 9. Snapshot of the last frame from the simulation of Melittin in HFIP/water. Only solvent molecules within 0.8 nm of any atom of Melittin are shown. HFIP molecules are represented by a sphere centered on the C$_c$ atom.

essentially identical to the crystallographic structure with slight fraying at the ends. The structure in water shows fraying at the ends and also in the middle. The extent of fraying at the ends and in the middle varies during the simulation.

Figure 9 shows a snapshot of the distribution of the HFIP molecules (represented by spheres centered on C_c atoms) around the Melittin molecule. In the simulation, the HFIP molecules cluster around the peptide forming a coat and reducing its mobility.

5. Conclusions

In this paper, a new model of HFIP for molecular dynamics simulations has been presented. The model was parametrized at 298 K to be compatible with the GROMOS96 force field. Overall, the thermodynamic and kinetic properties of the neat liquid calculated based on the model show reasonable to good agreement with the available experimental data. The shear viscosity of the model at 298 K is higher than the corresponding experimental value which could be a consequence of the strong network of hydrogen bonds formed in the pure liquid. The dielectric constant is underestimated, possibly a consequence of insufficient sampling and/or the absence of explicit polarization within the force field. The thermodynamic properties of the HFIP−water solutions were also investigated. The free energy of hydration shows a good agreement with the experimental value. The HFIP model is completely soluble with SPC water at all molar fractions. There is, nevertheless, evidence of microheterogeneity consistent with the results of SAXS experiments.[3] Simulations of the peptide Melittin in water and in 30% v/v HFIP, demonstrate that the solvent markedly stabilizes the α-helical conformation in agreement with experiment.[3] Work is in progress to investigate the nature of this phenomena further.

References and Notes

(1) Buck, M. *Q. Rev. Biophys.* **1998**, *31*, 297−355.

(2) Wood, S. J.; Maleeff, B.; Hart, T.; Wetzel, R. *J. Mol. Biol.* **1996**, *256*, 870−877.

(3) Hong, D.; Hoshino, M.; Kuboi, R.; Goto, Y. *J. Am. Chem. Soc.* **1999**, *121*, 8427−8433.

(4) Liu, Y.; Bolen, D. W. *Biochemistry* **1995**, *34*, 12884−12891.

(5) Hirota-Nakaoka, N.; Mizuno, K.; Goto, Y. *J. Mol. Biol.* **1998**, *275*, 365−368.

(6) Zhang, H.; Kaneko, K.; Nguyen, J. T.; Livshits, T. L.; Baldwin, M. A.; Cohen, F. E.; James, T. L.; Prusiner, S. B. *J. Mol. Biol.* **1995**, *250*, 514−526.

(7) Schaal, H.; Häber, T.; Suhm, M. A. *J. Phys. Chem.* **2000**, *104*, 265−274.

(8) Mizutani, Y.; Kinugawa, K.; Kitagawa, T.; Shimizu, A.; Taniguchi, Y.; Nakanishi, K. *J. Phys. Chem.* **1991**, *95*, 1790−1794.

(9) Kenichi, K.; Koiciro, N. *J. Chem. Phys.* **1988**, *89*, 5834−5842.

(10) van Gunsteren, W. F.; Billeter, S. R.; Eising, A. A.; Hünenberger, P. H.; Krüger, P.; Mark, A. E.; Scott, W. R. P.; Tironi, I. G. *Biomolecular Simulation: The GROMOS96 Manual and User Guide*; vdf Hochschulverlang ETH: Zürich, Switzerland, 1996.

(11) Berendsen, H. J. C.; Grigera, J. R.; Straatsma, T. P. *J. Chem. Phys.* **1987**, *91*, 6269−6271.

(12) Haberman, H. *Science* **1972**, *177*, 314−322.

(13) Frisch, M. J.; Trucks, G. W.; Schlegel, H. B.; Scuseria, G. E.; Robb, M. A.; Cheeseman, J. R.; Zakrzewski, V. G.; Montgomery, J. A., Jr.; Stratmann, R. E.; Burant, J. C.; Dapprich, S.; Millam, J. M.; Daniels, A. D.; Kudin, K. N.; Strain, M. C.; Farkas, O.; Tomasi, J.; Barone, V.; Cossi, M.; Cammi, R.; Mennucci, B.; Pomelli, C.; Adamo, C.; Clifford, S.; Ochterski, J.; Petersson, G. A.; Ayala, P. Y.; Cui, Q.; Morokuma, K.; Malick, D. K.; Rabuck, A. D.; Raghavachari, K.; Foresman, J. B.; Cioslowski, J.; Ortiz, J. V.; Stefanov, B. B.; Liu, G.; Liashenko, A.; Piskorz, P.; Komaromi, I.; Gomperts, R.; Martin, R. L.; Fox, D. J.; Keith, T.; Al-Laham, M. A.; Peng, C. Y.; Nanayakkara, A.; Gonzalez, C.; Challacombe, M.; Gill, P. M. W.; Johnson, B. G.; Chen, W.; Wong, M. W.; Andres, J. L.; Head-Gordon, M.; Replogle, E. S.; Pople, J. A. *Gaussian 98*, revision A.3; Gaussian, Inc.: Pittsburgh, PA, 1998.

(14) Fioroni, M.; Burger, K.; Mark, A. E.; Roccatano, D. *J. Phys. Chem. B* **2000**, *104*, 12347−12354.

(15) Marstokk, K. M.; Mollendall, H. *Acta Chem. Scand.* **1998**, *52*, 1307−1313.

(16) Spirig, N. Ph.D. Thesis, ETH Zurich, 1984.

(17) Murto, J.; Kivinen, A. *Suom. Kemistil. B* **1967**, *40*, 14−18.

(18) Breneman, C. M.; Wiberg, K. B. *J. Comput. Chem.* **1990**, *11*, 361−397.

(19) Carlson, H. A.; Nguyen, T. B.; Orozco, M.; Jorgensen, W. *J. Comput. Chem.* **1993**, *14*, 1240−1249.

(20) Berendsen, H. J. C.; Postma, J. P. M.; DiNola, A.; Haak, J. R. *J. Chem. Phys.* **1984**, *81*, 3684−3690.

(21) Mehta, S. K.; Sharma, A. K.; Parkash, R.; Chadha, S. L. *J. Chem. Soc., Faraday Trans.* **1998**, *49*, 2565−2569.

(22) Hess, B.; Bekker, H.; Berendsen, H. J. C.; Fraaije, J. G. E. M. *J. Comput. Chem.* **1997**, *18*, 1463−1472.

(23) Miyamoto, S.; Kollman, P. A. *J. Comput. Chem.* **1992**, *13*, 952−962.

(24) Allen, M. P.; Tildesley, D. J. *Computer Simulations of Liquids;* Oxford Science Publications: Oxford, U.K., 1987.

(25) Morishita, T. *J. Chem. Phys.* **2000**, *113*, 2976−2982.

(26) Anderson, D.; Terwilliger, T. C.; Wickner, W.; Eisenberg, D. *J. Biol. Chem.* **1980**, *255*, 2578−2582.

(27) Jarvis, R. A.; Patrick, E. A. *IEEE Trans. Comput.* **1973**, *22*, 1025−1034.

(28) van der Spoel, D.; Berendsen, H. J. C.; van Buuren, A. R.; Apol, E.; Meulenhoff, P. J.; Sijbers, A. L. T. M.; van Drunen, R. *Gromacs User Manual*; 1995. (http://www.gromacs.org/)

(29) Evans, A.; McElroy, G. *J. Solution Chem.* **1975**, *4*, 413−416.

(30) Walser, R.; Mark, A. E.; van Gunsteren, W. F. *J. Chem. Phys.* **1999**, *112*, 10450−10458.

(31) Mainar, A.; Pardo, J. G.; Jose, I.; Royo, F. M.; Urieta, J. *J. Chem. Soc., Faraday Trans.* **1998**, *24*, 3595−3600.

(32) Neumann, M. *Mol. Phys.* **1983**, *50*, 841−852.

(33) DeBolt, S. E.; Kollman, P. A. *J. Am. Chem. Soc.* **1995**, *117*, 5316−5340.

(34) Berendsen, H. J. C. Transport properties computed by linear response through weak coupling to a bath. In *Computer Simulations in Material Science*; Meyer, M.; Pontikis, V., Eds.; Kluwer: Dordrecht, The Netherlands, 1991.

(35) Feenstra, K. A.; Hess, B.; Berendsen, H. J. C. *J. Comput. Chem.* **1999**, *20*, 786−798.

(36) Marcus, Y. The Properties of Solvents. of *Wiley Series in Solution Chemistry*; John Wiley & Sons: New York, 1998; Vol. 4.

(37) van Gunsteren, W. F.; Daura, X.; Mark, A. E. Free Energy Perturbation Calculations. In *Encyclopaedia of Computational Chemistry 2*; von Rague Schleyer, P., Ed.; John Wiley & Sons: New York, 1998.

(38) Beutler, T. C.; Mark, A. E.; van Schaik, R. C.; Gerber, P. R.; van Gunsteren, W. F. *Chem. Phys. Lett.* **1994**, *222*, 529−539.

(39) Zacharias, M.; Straatsma, T. P.; McCammon, J. A. *J. Chem. Phys.* **1994**, *100*, 9025−9031.

(40) Daura, X.; Hünenberger, P. H.; Mark, A. E.; Querol, E.; Aviles, F. X.; van Gunsteren, W. F. *J. Am. Chem. Soc.* **1996**, *118*, 6285−6294.

(41) Cabani, S.; Gianni, P.; Mollica, V.; Lepori, L. *J. Solution Chem.* **1981**, *10*, 563−595.

(42) Blandamer, M. J.; Burgess, J.; Coonea, A.; Cowles, H. J.; Horn, M. I.; Martin, K. J.; Morcom, W. K.; Warrick, P. J. *J. Chem. Soc., Faraday Trans.* **1990**, *86*, 2209−2213.

(43) Müller-Plathe, F. *Mol. Simul.* **1996**, *18*, 133−143.

(44) Chitra, R.; Smith, P. E. *J. Chem. Phys.* **2001**, *114*, 426−435.

(45) Chitra, R.; Smith, P. E. *J. Phys. Chem. B* **2000**, *104*, 5854−5864.

(46) Mills, R. *J. Phys. Chem.* **1973**, *77*, 685−690.

(47) Lin, J. H.; Baumgaertner, A. *Comput. Theor. Polym. Sci.* **2000**, *10*, 97−102.

(48) Kraulis, P. J. *J. Appl. Cryst.* **1991**, *24*, 946−950.

(49) Kabsch, W.; Sander, C. *Biopolymers* **1983**, *22*, 2576−2637.